

Investigation of ensemble averaged maximal center gauge

Investigation of ensemble averaged maximal center gauge

Zeinab Dehghan,^{1, a)} Rudolf Golubich,^{2, b)} Roman Höllwieser,^{3, c)} and Manfried Faber^{2, d)}

¹⁾Department of Physics,

University of Tehran

²⁾Atominstitut,

Technische Universität Wien

³⁾Department of Physics,

Bergische Universität Wuppertal

(Dated: 18 January 2023)

Synopsis

To cure the problem of finding the global maximum of the gauge functional in maximal center gauge we present the Ensemble averaged Maximal Center Gauge (EaMCG). It allows for a vortex specific extraction of the quark-antiquark potential from an ensemble of gauge copies. Evaluating center projected Wilson loops we compare EaMCG with other center vortex based measurements of the string tension in SU(2).

Keywords: quantum chromodynamics; confinement; center vortex model; vacuum structure

I. INTRODUCTION

The fundamental role of center vortices in the ground-state vacuum fields governing the confinement of quarks and chiral symmetry breaking has been shown in Lattice QCD in the past decades^{1–13}. The *center vortex model* for quark-confinement assumes that closed quantised color-magnetic flux tubes percolating the QCD vacuum are responsible for a non-vanishing string tension. It explains confinement, topological charge and chiral symmetry breaking^{14–35} and reproduces the expected behavior of the string tension throughout a wide range of β -values, although the detection of center vortices in field configurations can be difficult.

The main methods to detect center vortices are based on Maximal Center Gauge (MCG)^{36–38} via maximizing an appropriate gauge functional R_{MCG} , usually restricted by an upper and lower limit which we can consider without loss of generality as $0 \leq R_{\text{MCG}} \leq 1$. It is not possible to numerically identify a global maximum and one can only consider an ensemble of gauge copies $\{\mathcal{C}_1, \mathcal{C}_2, \mathcal{C}_3, \dots, \mathcal{C}_n\}$ which can be seen as a partially ordered set $\mathcal{C}_1 \leq \mathcal{C}_2 \leq \mathcal{C}_3 \leq \dots \leq \mathcal{C}_n$ with respect to R_{MCG} . During an optimization procedure the physical interpretation of consecutive gauge copies can vary, but differences should decrease with the gauge functional approaching its maximal value. If they do not, one speaks of *Gribov ambiguities* or *Gribov problems* and care has to be taken when interpreting such gauge configurations.

We were able to solve the problems by usage of non-trivial center regions^{39–45}. Our solution does not perform the gauge fixing solely on a microscopic level (taking only single lattice points and the links attached to them into account) but requires the non-trivial center regions, macroscopic structures, to guide the gauge fixing procedure.

In this work we present a different approach that extracts the quark-antiquark potential from an ensemble of gauge copies, the *Ensemble averaged Maximal Center Gauge* (EaMCG). Motivated by our findings in⁴⁶ we look at a reasonable large ensemble of MCG copies with respect to the value of the gauge functional and the string tension. The method starts

^{a)}Electronic mail: zeinab.dehghan@ut.ac.ir

^{b)}Electronic mail: rudolf.golubich@gmail.com

^{c)}Electronic mail: hoellwieser@uni-wuppertal.de

^{d)}Electronic mail: faber@kph.tuwien.ac.at

with the production of the ensemble and executes on each single gauge copy a gradient climb towards the nearest local maximum of the gauge functional. After center projection, average values of Wilson loops $\langle W_{\text{CP}} \rangle$ and the quark-antiquark potentials are determined. This new method is compared in $\text{SU}(2)$ gauge theory to other center gauges such as *adjoint Laplacian Landau gauge* (ALLG) and *direct Laplacian Landau gauge* (DLCG) and to the potentials extracted from the unprojected (original) field configurations. The expected scaling behavior as predicted by renormalization group theory is reproduced.

II. METHODS AND FORMALISM: FROM CENTER GAUGES TO STRING TENSION IN LATTICE-QCD

We work on periodic lattices with $U_\mu(x) \in \text{SU}(2)$ denoting a gluonic link at lattice site x pointing in direction μ , where Wilson action

$$S_{\text{gluons}} = \beta \sum_{x, \mu < \nu} \left(1 - \frac{1}{2} \Re \text{Tr}(U_{\mu\nu}(x)) \right) \quad (1)$$

with $U_{\mu\nu}(x)$ corresponding to a plaquette in the plane spanned by the directions μ and ν is used in a Monte Carlo procedure. For the inverse coupling $\beta = \frac{4}{g^2}$ we choose $\beta = 2.3, 2.4, 2.5, 2.6, 2.7$.

Center vortices are usually detected in *direct maximal center gauge* (DMCG) that uses a gradient climb to identify the gauge transformation $g(x) \in \text{SU}(2)$ maximizing the gauge functional

$$R_{\text{MCG}} = \sum_x \sum_\mu | \text{Tr}[^g U_\mu(x)] |^2 \quad (2)$$

with ${}^g U_\mu(x) = g(x + \hat{\mu}) U_\mu(x) g^\dagger(x)$. Starting on multiple random gauge copies this procedure is executed and the gauge copy with the largest value of the gauge functional is taken for further processing: The link variables ${}^g U_\mu(x)$ are projected to the center degrees of freedom, that is ± 1 for $\text{SU}(2)$,

$${}^g U_\mu(x) \rightarrow Z_\mu(x) \equiv \text{sign} \text{Tr}[{}^g U_\mu(x)]. \quad (3)$$

The resulting non-trivial center projected plaquettes are known as *P-plaquettes*, $U_\square = -1$, which contain one or three non-trivial links. The duals of P-plaquettes form closed surfaces in the four dimensional dual lattice and the dual P-vortices correspond to the closed flux lines evolving in time. Center projection is the common ground of center detection methods, only the specific gauge fixing procedures vary. Since $\text{Tr} U \text{Tr} U^\dagger = \text{Tr} U_A + 1$, where

$$[U^A]_{ij} = \frac{1}{2} \text{Tr}[\sigma_i U \sigma_j U^\dagger] \quad (4)$$

is the adjoint representation, MCG also maximizes

$$R_{\text{AL}} = \sum_{x, \mu} \text{Tr}_A[{}^g U_\mu^A(x)], \quad (5)$$

the gauge functional of the Landau gauge in the adjoint representation, which is blind to center elements. Landau gauge finds the configuration closest to a trivial field configuration. Hence, the functionals R_{MCG} and R_{AL} may fail to detect vortices in smooth field configurations, especially in the continuum limit. As was raised by Engelhardt and Reinhardt⁹ in the context of continuum Yang-Mills theory a thin vortex gets singular in this limit and must fail to approach a smooth configuration.

Gauges not directly suffering from Gribov copies are Laplacian gauges which require to solve the lattice Laplacian eigenvalue problem. They were first applied in Laplacian

Landau gauge by Vink and Wiese⁴⁷ for the detection of Abelian monopoles and modified to Laplacian center gauge in^{48,49} for center vortices which requires solving the eigenvalue problem of the lattice Laplacian in the adjoint representation

$$D_{ij}(x, y) = \sum_{\mu} (2\delta_{xy}\delta_{ij} - [U_{\mu}^A(x)]_{ij}\delta_{y,x+\hat{\mu}} - [U_{\mu}^A(x - \hat{\mu})]_{ji}\delta_{y,x-\hat{\mu}}). \quad (6)$$

The three lowest eigenvectors of this Laplacian are combined to matrices $M(x)$ in *adjoint Laplacian Landau gauge* (ALLG) which maximizes the functional

$$R_{\text{ALLG}} = \sum_x \sum_{\mu} \text{Tr}[M^{\dagger}(x)U_{\mu}^A(x)M(x + \hat{\mu})] \quad (7)$$

with $M(x) \in SO(3)$ "on average", that is, with weakened orthogonality constrained $\langle M^{\dagger} \cdot M \rangle = 1$. Even if the solution of the eigenvalue problem is a unique procedure, small modifications of the configuration may lead to different eigenfunctions corresponding to different positions of vortices. The combination of ALLG followed by DMCG^{50,51} is referred to as *direct Laplacian center gauge* (DLCG).

In the Monte-Carlo runs on a 24^4 lattice we did for each $\beta \in \{2.3, 2.4, 2.5, 2.6, 2.7\}$ 20 random starts, 3000 initial sweeps and produced 1000 configurations with a distance of 100 sweeps. For these 20 000 configurations we determined the averages of unprojected Wilson loops. Due to the large computational needs we did center projection by ALLG, DLCG and EaMCG for every 100th of these 20 000 configurations only. For EaMCG we did 100 unbiased gauge copies for each of the 200 configurations. In Fig. 7 we compare the 24^4 data for unprojected configurations with the same number of analogously produced 32^4 configurations.

The problem of the gauge functional and its resolution

The gauge functional (2) has a huge number of local maxima and it is practically impossible to find the absolute maximum. The numeric maximization of the gauge functional suffers from a severe problem as was shown by Bornyakov, Komarov, and Polikarpov (BKP) in ref.⁵² with simulated annealing: The largest maxima of the functional underestimate the density of vortices and therefore also the string tension. Since there are only relatively few of these maxima it is rather tiresome to find them by simulated annealing.

Random gauge copies are usually determined by random gauge matrices $g(x)$ with a homogeneous density on the $SU(2)$ group manifold, as produced by the Box-Muller method⁵³. One can get directly to consecutively increasing local maxima of the gauge functional by a bias in these random gauge transformations by restricting the gauge transformation to the hemisphere of $SU(2) \cong \mathbb{S}^3$ with positive trace. In the two diagrams in Fig. 1 we show the maximizing histories for two independently created field configurations (out of 200) and for ten of their random gauge copies. For each of these 20 field configurations we perform 100 times the following two steps: First, we maximize the functional by gradient climb. Secondly, we apply the biased random gauge transformations. For center projected field configurations of sufficient large lattice size already one configuration can result in reasonable values of Creutz-ratios

$$\sigma \approx \chi_{\text{CP}}(R) = -\ln \frac{W_{\text{CP}}(R+1, R+1)}{W_{\text{CP}}(R, R+1)} \frac{W_{\text{CP}}(R, R)}{W_{\text{CP}}(R+1, R)}, \quad (8)$$

for small Wilson loops $W_{\text{CP}}(R, T)$ of size $R \times T$, which are averages over the center projected configurations of the ensemble. In Fig. 1 we show $\chi_{\text{CP}} - R_{\text{MCG}}$ pairs for the evolution through the biased gauge fixing iterations. A nearly linear relation between χ_{CP} and R_{MCG} can be observed. With increasing gauge functional we observe a linear decrease of the string tension, underestimating the expected value of $\sigma = 0.0350(12)$ ⁵⁴. With this method we did not find any configuration where the maximum of the gauge functional did not

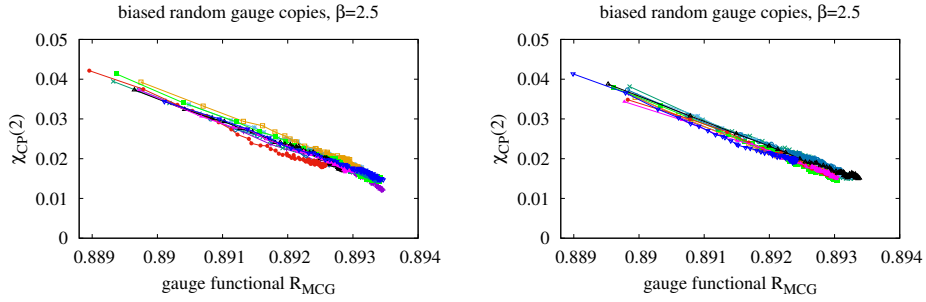


FIG. 1: In the two diagrams we show the maximizing histories of two independent field configurations on a 24^4 lattice for ten random gauge copies each. Interchanging hundred times gradient climbs and biased random gauge transformations we get hundred points in the $\chi_{CP} - R_{MCG}$ plane connected by a line. Observe the nearly linear relation between Creutz ratio χ_{CP} and gauge functional R_{MCG} and especially the final low value of χ_{CP} , much lower than the expected string tension $\sigma = 0.035$.

dramatically underbid the string tension. On the other hand, DMCG^{6,55} predicts the string tension very successfully using a few gauge copies and choosing the one with the highest value of the functional for further analysis. This demonstrates the physical relevance of the gauge functional and implies that it is the prescription for global maximization which is problematic. In DLCG^{50,51} the mentioned problems were circumvented using the eigenfunctions of the adjoint Laplacian operator to select a smooth gauge field before maximizing the gauge functional in a gradient climb. In this article we investigate a different approach: *ensemble averaged maximal center gauge* (EaMCG). We produce random gauge copies with the correct \mathbb{S}^3 -weight, approach the next local maximum by the gradient method and take the average of an ensemble of such random gauge copies. The idea is that not the best local maximum alone carries the physical information but the average over all local maxima does: maxima with a higher value of the gauge functional result in a reduced string tension, but they do not dominate the ensemble. The same holds for lower valued maxima, possibly overestimating the string tension. This method is strengthened by density plots of 20 000 $R_{MCG}/\chi_{CP}(2)$ pairs in Fig. 2 for $\beta \in \{2.3, 2.4, 2.5, 2.6, 2.7\}$. For all β -values we see a clear linear correlation as expected from Fig. 1. The average slope of the distributions agrees in both figures. The β -dependence of the elliptic distributions is a running coupling effect. With increasing β , higher Creutz ratios can be resolved, but give broader distributions due to larger statistical errors. The average values of the distributions are marked by a “ \star ” and give first estimates of the string tension. From the type of distributions shown in Fig. 2 it gets understandable that the gauge configurations with extremely high functional (2) do not really contribute to the average. According to Eq. (8) Creutz ratios are determined from almost symmetric Wilson loops which are polluted by higher excitations and give therefore less confidential values for the string tension than the potential, extracted from maximally asymmetric Wilson loops with good signals as we will describe in the next section.

Extracting the string tension from Wilson loop data with the 1-exp-fit

We extract the static quark-antiquark potential from asymmetric $R \times T$ Wilson loops of an ensemble of configurations

$$\langle W(R, T) \rangle = \sum_{i=0}^{\infty} c_i e^{-\varepsilon_i(R)T}. \quad (9)$$

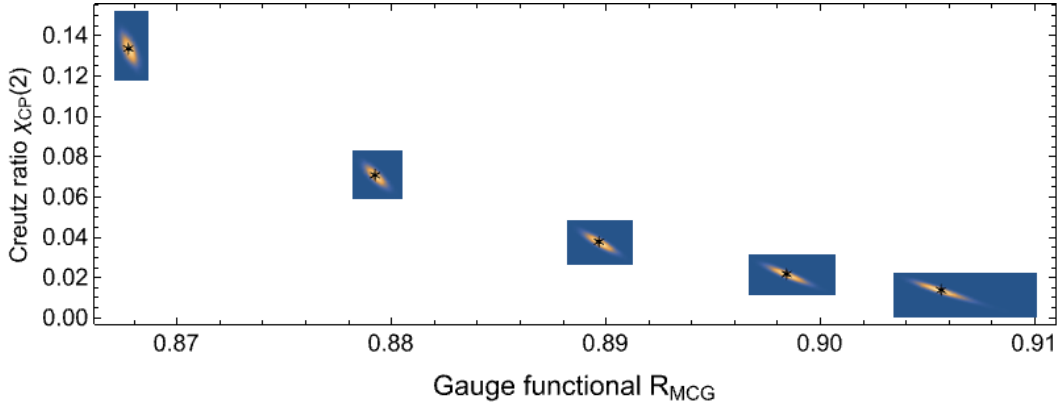


FIG. 2: Correlations between Creutz ratios $\chi_{CP}(2)$ and the values of the maximized gauge functionals R_{MCG} for center projected configurations for $\beta \in \{2.3, 2.4, 2.5, 2.6, 2.7\}$. On a 24^4 -lattice we produced the density plots with 20 random starts and 10 configurations with a distance of 10000 MC iterations and 100 gauge copies each. For each β the average values are marked by a star.

Only for the lowest states the amplitudes c_i and energies ε_i are resolvable. In Fig. 3 the logarithms of Wilson loops are shown at $\beta = 2.5$ comparing a 3-exp fit of original Wilson loops, a 2-exp fit of ALLG center projected loops, a 1-exp fit of DLCG based loops and 1-exp fit of EaMCG averaged loops. The curvature of original Wilson loops at small T is due to excited states that are almost eliminated in DLCG and EaMCG.

The larger the excitation energy, the more are excited states exponentially suppressed with increasing T . Finally, when the Wilson loops remain resolvable, only the ground state survives. To determine the ground state energy $\varepsilon_0(R)$ we introduce for each R an initial T_i and define a one-exponential fitting function (1-exp fit) for Wilson loops with $T \geq T_i$ as

$$\langle W(R, T) \rangle = c(R, T_i) e^{-\varepsilon_0(R, T_i) T}. \quad (10)$$

By removing small T s we observe that $\varepsilon_0(R, T_i)$ gets nearly stable in a fit range $T_i \approx T_{\text{opt}}$, the plateau region. T_{opt} is a function of R and therefore the plateau region has to be investigated for each R separately.

Keeping numerical issues under control proofs quite difficult: The Wilson loop averages from a single configuration are disturbed by noise, hence multiple configurations are averaged into $\langle W(R, T) \rangle$. The data is still disturbed by systematic errors resulting from unwanted higher excitations and statistical errors with increasing loop sizes: a decrease of the systematic error is accompanied by an increase of the statistical error. Therefore, the optimal T_i value, T_{opt} , we determine increasing T_i from the first local minimum of an error quantifier⁴⁶,

$$\text{Err} = \frac{2}{3} \langle \Delta_{\delta i} \rangle + \frac{1}{3} \langle \Delta_{\text{err}} \rangle \quad (11)$$

with $\langle \Delta_{\delta i} \rangle$ being the average change of the fit variable $\varepsilon_0(R, T_i)$ from previous to present T_{opt} and from present to next T_{opt} and $\langle \Delta_{\text{err}} \rangle$ being the average error of the respective three data points $\varepsilon(R, T_{i-1})$, $\varepsilon(R, T_i)$ and $\varepsilon(R, T_{i+1})$. Fig. 4 depicts some examples for the T_i dependence of $\varepsilon_0(R, T_i)$ and the chosen T_{opt} for $\beta = 2.5$ and some R for unprojected SU(2) configurations, ALLG, DLCG and EaMCG. For unprojected configurations and also for ALLG the excited states contribute at small distances and $\varepsilon_0(R, T_{\text{opt}}(R))$ is therefore approached from above. We observed in Fig. 3 that center projection for DLCG and EaMCG suppresses the excited states, the variations of ε_0 are therefore much smaller.

Once, $\varepsilon_0(R, T_{\text{opt}})$ is determined, we can identify it with the potential

$$V_W(R) = \varepsilon_0(R, T_{\text{opt}}(R)) \quad (12)$$

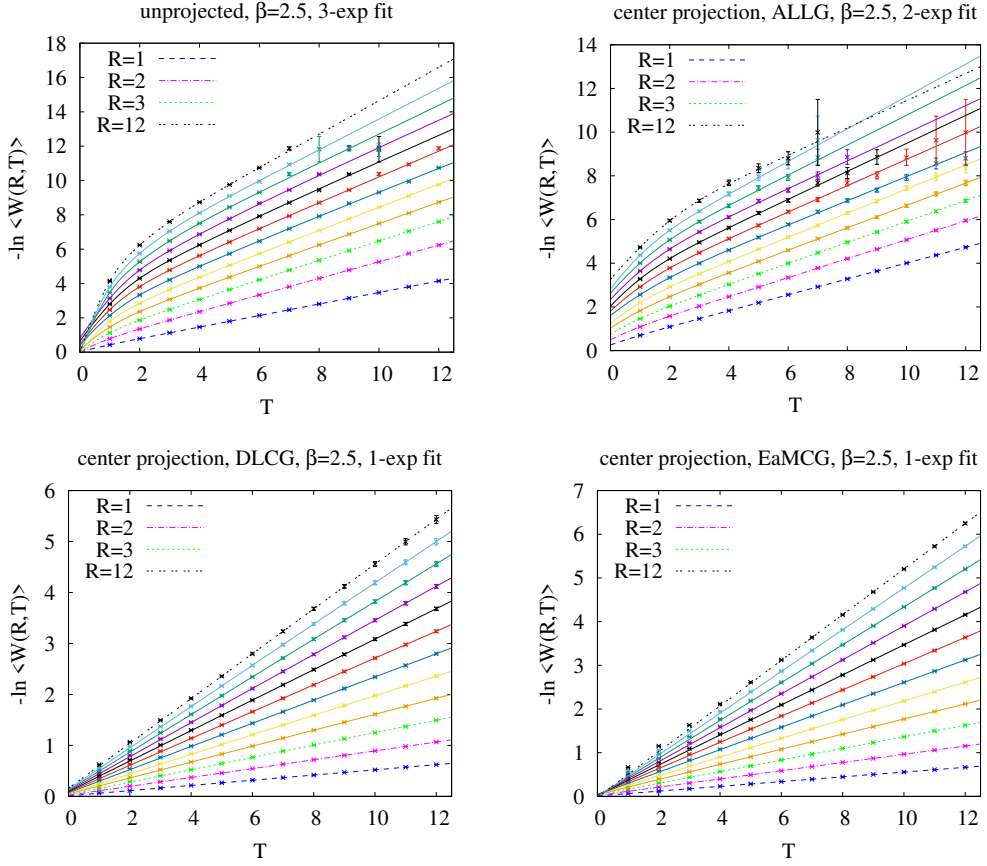


FIG. 3: A comparison of logarithms of Wilson loop data is depicted at $\beta = 2.5$ for original and projected configurations using different gauge fixing procedures. Observe that excited states contribute for large R essentially for unprojected configurations, less for ALLG and very little for DLCG and EaMCG.

extracted from Wilson loops.

III. RESULTS AND DISCUSSION

A. Center Dominance and Precocious Linearity

In this section, we compare the potentials extracted from original configurations with those which we get after center projections, especially with the main subject of this article with ensemble averaged maximal center gauge, EaMCG. To extract the physical parameters of the gluonic quark-antiquark string we fit the potentials $V_W(R)$ of Eq. (12) with a Cornell type of potential

$$V(R) = v_0 + \sigma R - \frac{c}{R} \quad (13)$$

with three parameters, self energy v_0 , string tension σ and Coulomb coefficient c . For original and ALLG configurations we need all three parameters. For DLCG and EaMCG we observe the feature of precocious linearity; i.e. the fact that the Coulombic term is strongly suppressed. Therefore we choose $c = 0$ and start the fit at some R_i .

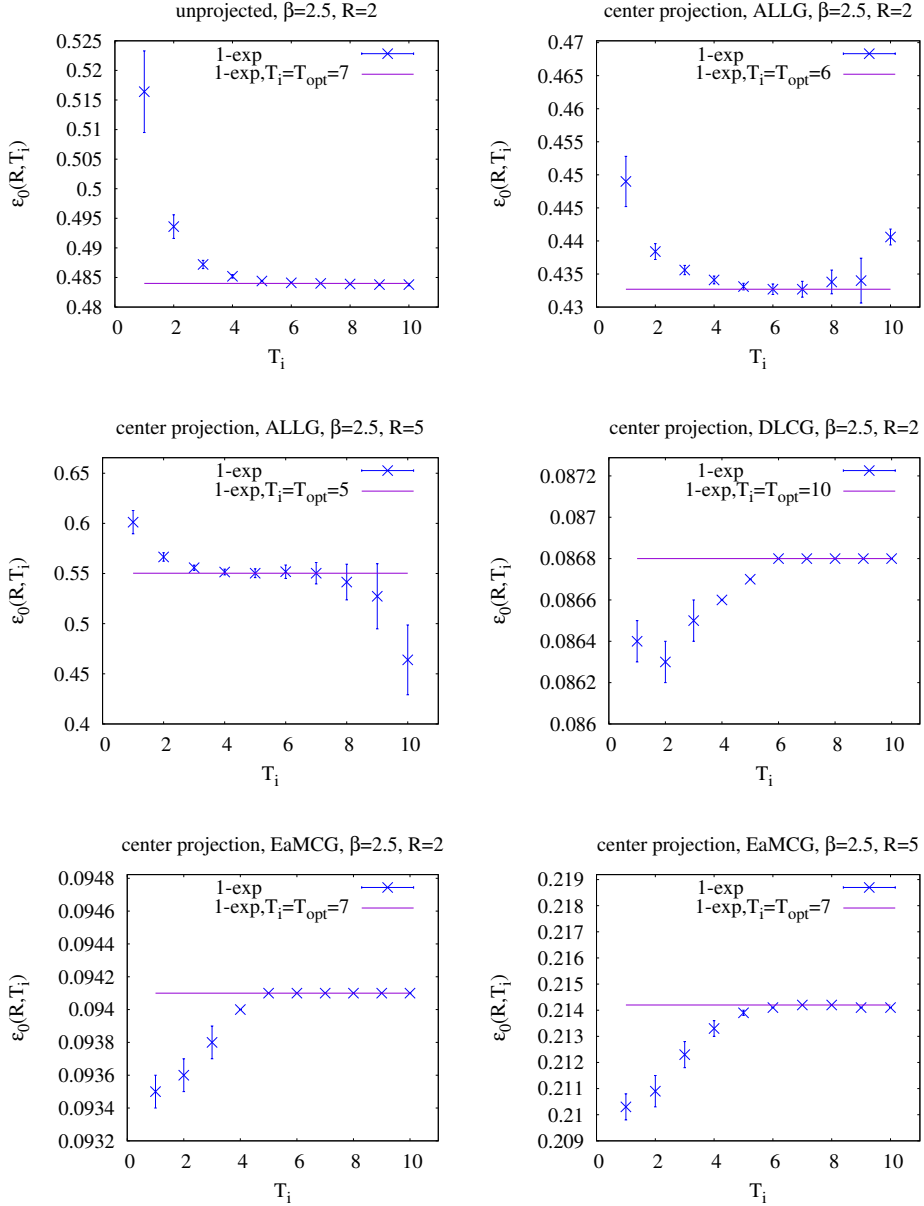


FIG. 4: Some examples of the T_i dependence of $\varepsilon_0(R, T_i)$ are shown. The final values at T_{opt} are depicted by horizontal lines. For original Wilson loops and ALLG, $\varepsilon_0(R, T_{\text{opt}}(R))$ is approached from above for $T_i \rightarrow T_{\text{opt}}$ due to the decaying contributions of excited states. Observe that for DLCG and EaMCG the variations of $\varepsilon_0(R, T_i)$ are much smaller since the lines in the lower part of Fig. 3 are remarkably straight.

For $\beta = 2.5$ we show in Fig. 5 the potential $V_W(R)$ of unprojected configurations, the fit potential $V(R)$, its contributions $v_0 - \frac{c}{R}$ and $v_0 + \sigma R$ together with the data of Ref.⁵⁴. We compare them with the potentials and their fits resulting from the three center projection methods, ALLG, DLCG and EaMCG. ALLG has a sizeable Coulomb contribution, differing in this respect from DLCG and EaMCG. ALLG leads to confidential values in the same region as $V_W(R)$. The potential is more difficult to resolve than for DLCG and EaMCG. ALLG has a smaller linear term than DLCG, where this term agrees nicely with the linear

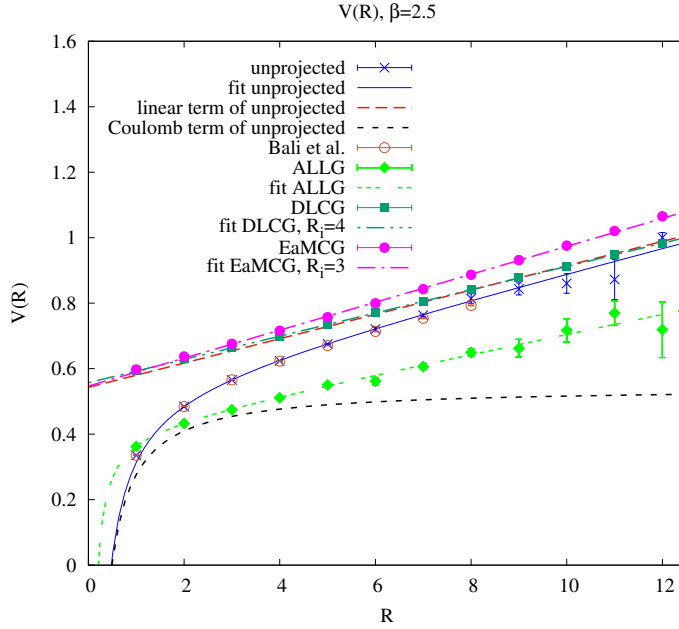


FIG. 5: For $\beta = 2.5$ on a 24^4 lattice, potentials determined with different methods are shown and compared to Ref⁵⁴. To ease comparisons, the potentials of EaMCG and DLCG are shifted by the self energy v_0 of the potential extracted from unprojected configurations.

term of the unprojected configurations. Over the whole R region the EaMCG values are very well resolvable and start at $R_i = 3$ to predict a stable value for the string tension σ . It is interesting to observe in Fig. 5 that, despite the linear term is larger than for DLCG and the unprojected configurations, the potential runs at large R nicely parallel to the unprojected potential. Since the Coulomb factor of the unprojected configurations is nearly proportional to $\pi/12$ and thus mainly due to string shape fluctuations this may be an indication that on the finite periodic lattice, in average, vortices do follow the shape fluctuations of the gluonic string. This behavior is reproduced for all tested values of β as can be seen in Fig. 6.

The parameters of the potentials are summarized in table I. The indicated errors are the statistical errors only. The systematic errors are difficult to quantify, but they are at least of the same size as the statistical errors as we can see comparing the data.

B. Scaling behavior

The string tension is expected to be proportional to the square of the lattice spacing a . For the SU(2) gauge group in the quenched approximation⁵⁶ asymptotic freedom predicts in two-loop order

$$a^2 = \frac{1}{\Lambda_L^2} \left(\frac{6\pi^2\beta}{11} \right)^{102} \exp\left(-\frac{6\pi^2}{11}\beta\right), \quad (14)$$

where Λ_L is the standard lattice scale parameter. In Fig. 7 we compare the string tensions extracted from unprojected and center projected configurations of Table I with the asymptotic freedom prediction. The main diagram shows the results of our calculations on a 24^4 lattice. In the insets we show fits to the asymptotic behavior $a^2 \propto \exp(-\frac{6\pi^2}{11}\beta)$, in the upper inset for EaMCG and in the lower inset for unprojected configurations on a

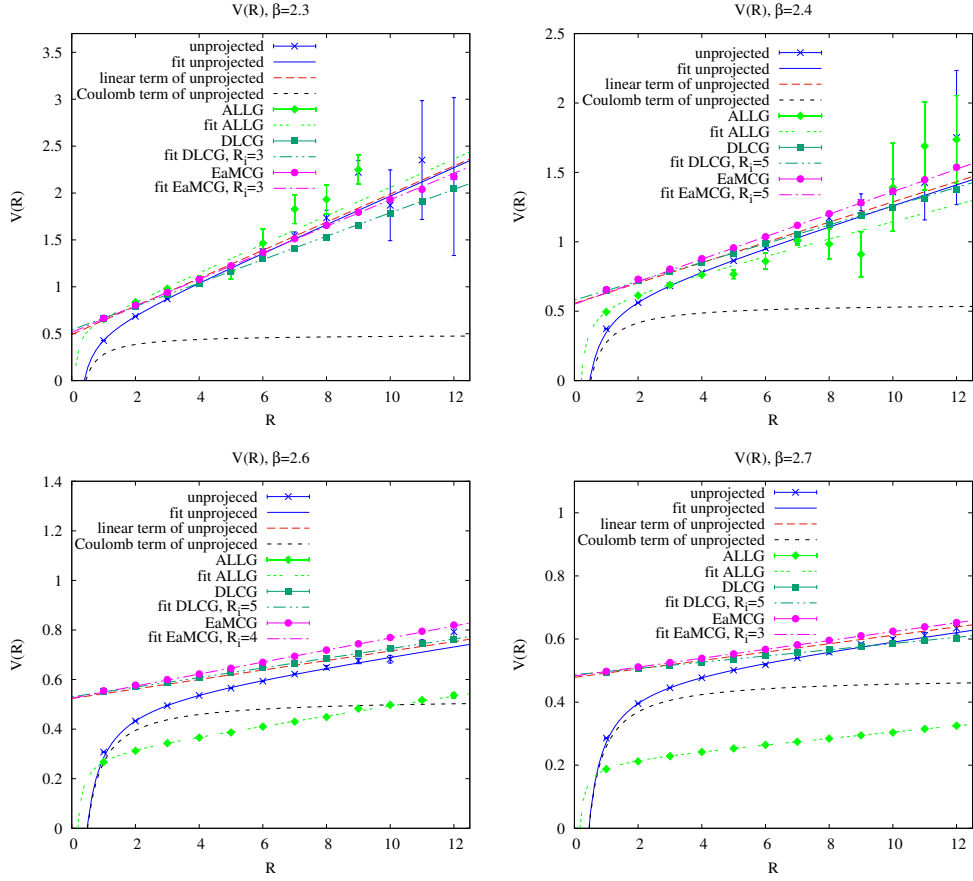


FIG. 6: For $\beta \in \{2.3, 2.4, 2.6, 2.7\}$ on a 24^4 lattice, the different methods to extract potentials and string tension are compared. For better visual comparison, the potentials of EaMCG and DLCG are shifted by the self energies of potentials extracted from original configurations.

32^4 lattice which scale much better than 24^4 data. We can clearly see in the insets that EaMCG and unprojected show the same scaling behavior and that EaMCG scales better than ALLG and DLCG.

IV. CONCLUSION

Center gauge methods suffer from the large differences between the center projected and unprojected configurations. These differences appear especially in the region of center vortices. Maximizing the center blind gauge functional (2) favors therefore to overlook vortices and to underestimate the string tension. This property is the basis of an approximate linear relation between the gauge functional and the string tension as shown in Figs. 1 and 2. This is a clear indication that the request for a global maximization of the gauge functional is not only difficult but erroneous.

Previously, there were two suggestions to overcome this failure of the global maximization condition. The first idea^{50,51} was to preselect a region of smooth gauge configurations where we maximize the gauge functional. With the three lowest eigenfunctions of the center blind lattice Laplacian in the adjoint representation we defined in ALLG a smooth gauged transformed configuration to start the maximization procedure by a gradient climb and to arrive at DLCG. In^{39,41,43} we suggested a completely different, but computationally rather involved approach, where we proposed to use global structures, non-trivial center

method	v_0	σ	c
$\beta = 2.3$			
unprojected, 24^4	0.492(8)	0.1496(27)	0.214(6)
unprojected, 24^4 , fix c	0.5289(43)	0.1431(21)	$\pi/12$
unprojected, 32^4	0.495(5)	0.1490(16)	0.216(3)
Z_2 , ALLG	0.557(66)	0.1508(193)	0.053(48)
Z_2 , DLCG	0.0496(18)	0.1247(6)	—
Z_2 , EaMCG	0.0237(13)	0.1412(4)	—
$\beta = 2.4$			
unprojected, 24^4	0.557(15)	0.0730(25)	0.284(20)
unprojected, 24^4 , fix c	0.5472(41)	0.0741(12)	$\pi/12$
unprojected, 32^4	0.552(10)	0.0728(17)	0.271(13)
Z_2 , ALLG	0.547(22)	0.0608(56)	0.112(16)
Z_2 , DLCG	0.0233(17)	0.0676(3)	—
Z_2 , EaMCG	-0.0070(21)	0.0811(4)	—
$\beta = 2.5$			
unprojected, 24^4	0.543(5)	0.0371(8)	0.266(6)
unprojected, 24^4 , fix c	0.5410(16)	0.0373(5)	$\pi/12$
unprojected, 32^4	0.552(5)	0.0350(8)	0.276(6)
Z_2 , ALLG	0.413(3)	0.0299(7)	0.081(2)
Z_2 , DLCG	0.01423(9)	0.03550(2)	—
Z_2 , EaMCG	0.0040(14)	0.0427(3)	—
$\beta = 2.6$			
unprojected, 24^4	0.524(4)	0.0191(6)	0.258(5)
unprojected, 24^4 , fix c	0.5256(12)	0.0189(3)	$\pi/12$
unprojected, 32^4	0.518(3)	0.0200(5)	0.251(4)
Z_2 , ALLG	0.302(2)	0.0197(5)	0.054(2)
Z_2 , DLCG	0.00655(11)	0.01946(2)	—
Z_2 , EaMCG	0.0013(8)	0.0242(2)	—
$\beta = 2.7$			
unprojected, 24^4	0.479(3)	0.0133(5)	0.219(5)
unprojected, 24^4 , fix c	0.4951(31)	0.0118(7)	$\pi/12$
unprojected, 32^4	0.489(2)	0.0116(3)	0.234(3)
Z_2 , ALLG	0.211(1)	0.0097(2)	0.034(2)
Z_2 , DLCG	0.00822(34)	0.00988(6)	—
Z_2 , EaMCG	0.0042(2)	0.01406(6)	—

TABLE I: The parameters, string tension σ , self energy v_0 and Coulomb factor c , of the fitting potential (13) are compared for the various methods.

regions, to guide the gauge fixing procedure. These two successful methods indicate that the failure of Direct Maximal Center Gauge was in the prescription to determine the global maximum of the gauge functional. In the new method suggested in this article, ensemble averaged maximal center gauge (EaMCG), we are using the physical information contained in the huge ensemble of local maxima of the functional. The gluon string between a static quark-antiquark pair with large separation fluctuates leading to a Coulombic contribution proportional to $\pi/12^{57}$. Projected vortices follow these fluctuations leading to an increase of the P-vortex area compared to a straight string and result in a slightly larger string tension than DLCG. The potential extracted from these areas follows nicely the large distance behavior of the string on a finite periodic lattice.

Recently, an improved method for computing the static quark-anti-quark potential in lattice QCD was investigated in^{58–60}, which is not based on Wilson loops, but formulated in terms of (temporal) *Laplace trial state correlators*, formed by eigenvector components of the covariant lattice Laplace operator. This approach seems very promising and an application to center vortex configurations as well as a generalization of the methods introduced in this article to $SU(3)$ is left for future investigations.

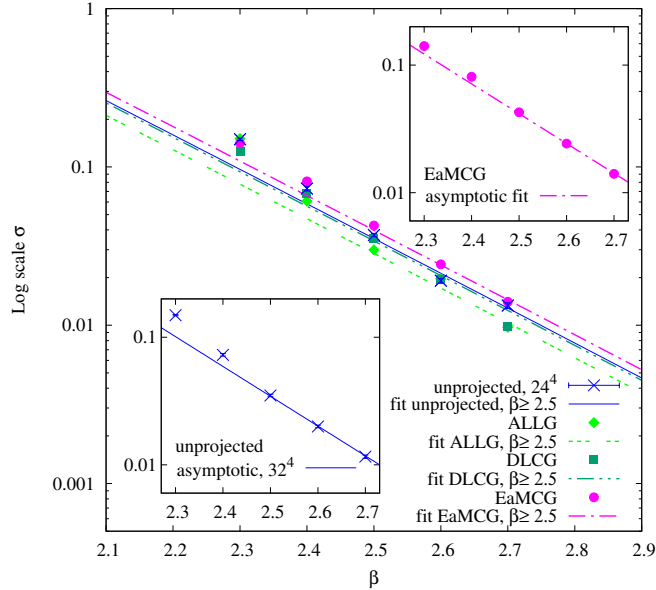


FIG. 7: The dependence of string tensions extracted from unprojected and center projected configurations on β are compared with the predictions of asymptotic freedom. For each of the methods the lattice scale parameter Λ_L is adjusted separately to the data with $\beta \geq 2.5$.

ACKNOWLEDGEMENTS

The authors gratefully acknowledge the Vienna Scientific Cluster (VSC) for providing supercomputer resources. R.H. was supported by the MKW NRW under the funding code NW21-024-A. We thank Sedigheh Deldar for valuable discussions.

REFERENCES

- ¹Gerard 't Hooft. On the Phase Transition Towards Permanent Quark Confinement. *Nucl. Phys. B*, 138: 1–25, 1978. doi:10.1016/0550-3213(78)90153-0.
- ²Gerard 't Hooft. A Property of Electric and Magnetic Flux in Nonabelian Gauge Theories. *Nucl. Phys. B*, 153:141–160, 1979. doi:10.1016/0550-3213(79)90595-9.
- ³John M. Cornwall. Quark confinement and vortices in massive gauge-invariant qcd. *Nuclear Physics B*, 157(3):392 – 412, 1979. ISSN 0550-3213. doi:https://doi.org/10.1016/0550-3213(79)90111-1. URL <http://www.sciencedirect.com/science/article/pii/0550321379901111>.
- ⁴L. Del Debbio, M. Faber, J. Greensite, and Š. Olejník. Center dominance and $Z(2)$ vortices in $SU(2)$ lattice gauge theory. *Phys. Rev.*, D55:2298–2306, 1997. doi:10.1103/PhysRevD.55.2298.
- ⁵Manfried Faber, J. Greensite, and S. Olejnik. Casimir scaling from center vortices: Towards an understanding of the adjoint string tension. *Phys. Rev. D*, 57:2603–2609, 1998. doi:10.1103/PhysRevD.57.2603.
- ⁶L. Del Debbio, Manfried Faber, J. Giedt, J. Greensite, and S. Olejnik. Detection of center vortices in the lattice Yang-Mills vacuum. *Phys. Rev. D*, 58:094501, 1998. doi:10.1103/PhysRevD.58.094501.
- ⁷R. Bertle, Manfried Faber, J. Greensite, and S. Olejnik. The Structure of projected center vortices in lattice gauge theory. *JHEP*, 03:019, 1999. doi:10.1088/1126-6708/1999/03/019.
- ⁸Manfried Faber, J. Greensite, S. Olejnik, and Daisuke Yamada. The Vortex finding property of maximal center (and other) gauges. *JHEP*, 12:012, 1999. doi:10.1088/1126-6708/1999/12/012.
- ⁹M. Engelhardt and H. Reinhardt. Center projection vortices in continuum yang-mills theory. *Nucl. Phys.*, B567:249, 2000.
- ¹⁰Roman Bertle, Manfried Faber, Jeff Greensite, and Stefan Olejnik. P vortices, gauge copies, and lattice size. *JHEP*, 10:007, 2000. doi:10.1088/1126-6708/2000/10/007.
- ¹¹J. Greensite. The Confinement problem in lattice gauge theory. *Prog. Part. Nucl. Phys.*, 51:1, 2003. doi:10.1016/S0146-6410(03)90012-3.
- ¹²M. Engelhardt, M. Quandt, and H. Reinhardt. Center vortex model for the infrared sector of $SU(3)$ Yang-Mills theory: Confinement and deconfinement. *Nucl. Phys. B*, 685:227–248, 2004. doi:

- 10.1016/j.nuclphysb.2004.02.036.
- ¹³Jeff Greensite. Confinement from Center Vortices: A review of old and new results. *EPJ Web Conf.*, 137:01009, 2017. doi:10.1051/epjconf/201713701009.
- ¹⁴Philippe de Forcrand and Massimo D'Elia. On the relevance of center vortices to QCD. *Phys. Rev. Lett.*, 82:4582–4585, 1999. doi:10.1103/PhysRevLett.82.4582.
- ¹⁵C. Alexandrou, P. de Forcrand, and Massimo D'Elia. The Role of center vortices in QCD. *Nucl. Phys.*, A663:1031–1034, 2000. doi:10.1016/S0375-9474(99)00763-0.
- ¹⁶H. Reinhardt and M. Engelhardt. Center vortices in continuum yang-mills theory. In Wolfgang Lucha and Khin Maung Maung, editors, *Quark Confinement and the Hadron Spectrum IV*, pages 150–162. World Scientific, 2002.
- ¹⁷Michael Engelhardt. Center vortex model for the infrared sector of Yang-Mills theory: Quenched Dirac spectrum and chiral condensate. *Nucl. Phys.*, B638:81–110, 2002. doi:10.1016/S0550-3213(02)00470-4.
- ¹⁸V. G. Bornyakov, E. -M. Ilgenfritz, B. V. Martemyanov, S. M. Morozov, M. Müller-Preussker, and A. I. Veselov. Interrelation between monopoles, vortices, topological charge and chiral symmetry breaking: Analysis using overlap fermions for SU(2). *Phys. Rev.*, D77:074507, 2008. doi:10.1103/PhysRevD.77.074507.
- ¹⁹R. Höllwieser, M. Faber, J. Greensite, U. M. Heller, and Š. Olejník. Center Vortices and the Dirac Spectrum. *Phys. Rev.*, D78:054508, 2008. doi:10.1103/PhysRevD.78.054508.
- ²⁰R. Höllwieser, M. Faber, U. M. Heller. Intersections of thick Center Vortices, Dirac Eigenmodes and Fractional Topological Charge in SU(2) Lattice Gauge Theory. *JHEP*, 06:052, 2011. doi:10.1007/JHEP06(2011)052.
- ²¹T. Schweigler, R. Höllwieser, M. Faber, and U. M. Heller. Colorful SU(2) center vortices in the continuum and on the lattice. *Phys. Rev.*, D87(5):054504, 2013. doi:10.1103/PhysRevD.87.054504.
- ²²R. Höllwieser, M. Faber, and U.M. Heller. Critical analysis of topological charge determination in the background of center vortices in SU(2) lattice gauge theory. *Phys. Rev.*, D86:014513, 2012. doi:10.1103/PhysRevD.86.014513.
- ²³R. Höllwieser, T. Schweigler, M. Faber, and U. M. Heller. Center Vortices and Chiral Symmetry Breaking in SU(2) Lattice Gauge Theory. *Phys. Rev.*, D88:114505, 2013. doi:10.1103/PhysRevD.88.114505.
- ²⁴R. Höllwieser, M. Faber, T. Schweigler, and U. M. Heller. Chiral Symmetry Breaking from Center Vortices. *PoS*, LATTICE2013:505, 2014.
- ²⁵R. Höllwieser, and M. Engelhardt. Smearing Center Vortices. *PoS*, LATTICE2014:356, 2015.
- ²⁶R. Höllwieser, D. Altarawneh, and M. Engelhardt. Random center vortex lines in continuous 3D space-time. *AIP Conf. Proc.*, 1701:030007, 2016. doi:10.1063/1.4938613.
- ²⁷J. Greensite, and R. Höllwieser. Double-winding Wilson loops and monopole confinement mechanisms. *Phys. Rev.*, D91(5):054509, 2015. doi:10.1103/PhysRevD.91.054509.
- ²⁸R. Höllwieser, and M. Engelhardt. Approaching $SU(2)$ gauge dynamics with smeared $Z(2)$ vortices. *Phys. Rev.*, D92(3):034502, 2015. doi:10.1103/PhysRevD.92.034502.
- ²⁹Daniel Trewartha, Waseem Kamleh, and Derek Leinweber. Evidence that centre vortices underpin dynamical chiral symmetry breaking in $SU(3)$ gauge theory. *Phys. Lett.*, B747:373–377, 2015. doi:10.1016/j.physletb.2015.06.025.
- ³⁰R. Höllwieser, and D. Altarawneh. Center Vortices, Area Law and the Catenary Solution. *Int. J. Mod. Phys.*, A30(34):1550207, 2015. doi:10.1142/S0217751X15502073.
- ³¹D. Altarawneh, R. Höllwieser, and M. Engelhardt. Confining Bond Rearrangement in the Random Center Vortex Model. *Phys. Rev.*, D93(5):054007, 2016. doi:10.1103/PhysRevD.93.054007.
- ³²D. Altarawneh, M. Engelhardt, and R. Höllwieser. Model of random center vortex lines in continuous $2+1$ -dimensional spacetime. *Phys. Rev.*, D94(11):114506, 2016. doi:10.1103/PhysRevD.94.114506.
- ³³Daniel Trewartha, Waseem Kamleh, and Derek Leinweber. Centre vortex removal restores chiral symmetry. *J. Phys.*, G44(12):125002, 2017. doi:10.1088/1361-6471/aa9443.
- ³⁴Manfried Faber and Roman Höllwieser. Chiral symmetry breaking on the lattice. *Prog. Part. Nucl. Phys.*, 97:312–355, 2017. doi:10.1016/j.ppnp.2017.08.001.
- ³⁵James C. Biddle, Waseem Kamleh, and Derek B. Leinweber. Gluon propagator on a center-vortex background. *Phys. Rev.*, D98(9):094504, 2018. doi:10.1103/PhysRevD.98.094504.
- ³⁶L. Del Debbio, M. Faber, J. Greensite, and Š. Olejník. Center dominance and $Z(2)$ vortices in $SU(2)$ lattice gauge theory. *Phys. Rev. D*, 55:2298–2306, 1997. doi:10.1103/PhysRevD.55.2298.
- ³⁷Kurt Langfeld, Hugo Reinhardt, and Oliver Tennert. Confinement and scaling of the vortex vacuum of $SU(2)$ lattice gauge theory. *Phys. Lett.*, B419:317–321, 1998. doi:10.1016/S0370-2693(97)01435-4.
- ³⁸Kurt Langfeld. Vortex structures in pure $SU(3)$ lattice gauge theory. *Phys. Rev.*, D69:014503, 2004. doi:10.1103/PhysRevD.69.014503.
- ³⁹Rudolf Golubich and Manfried Faber. A possible resolution to troubles of $su(2)$ center vortex detection in smooth lattice configurations. *Universe*, 2021. doi:10.3390/universe7050122. URL <http://doi.org/10.3390/universe7050122>.
- ⁴⁰Rudolf Golubich and Manfried Faber. Properties of $su(2)$ center vortex structure in smooth configurations. *Particles*, 2021. doi:10.3390/particles4010011. URL <http://doi.org/10.3390/particles4010011>.
- ⁴¹R. Golubich and M. Faber. Center regions as a solution to the gribov problem of the center vortex model. *Acta Physica Polonica B Proceedings Supplement*, 14(1):87, 2021. doi:10.5506/aphyspolbsupp.14.87. URL <https://doi.org/10.5506/2Faphyspolbsupp.14.87>.

- ⁴²Rudolf Golubich and Manfried Faber. Thickness and color structure of center vortices in gluonic SU(2) QCD. *Particles*, 3(2):444–455, may 2020. doi:10.3390/particles3020031. URL <https://doi.org/10.3390/particles3020031>.
- ⁴³Rudolf Golubich. The road to solving the gribov problem of the center vortex model in quantum chromodynamics. *Acta Physica Polonica B Proceedings Supplement*, 2020. ISSN 2082-7865. doi: 10.5506/APhysPolBSupp.13.59. URL <http://doi.org/10.5506/APhysPolBSupp.13.59>.
- ⁴⁴Rudolf Golubich and Manfried Faber. Improving center vortex detection by usage of center regions as guidance for the direct maximal center gauge. *Particles*, 2019. doi:10.3390/particles2040030. URL <http://doi.org/10.3390/particles2040030>.
- ⁴⁵Rudolf Christopher Franz Golubich. *Improvement of vortex detection in SU (2)-QCD*. PhD thesis, Technische Universität Wien, 2022.
- ⁴⁶Zeinab Dehghan, Sedigheh Deldar, Manfried Faber, Rudolf Golubich, and Roman Höllwieser. Influence of fermions on vortices in su(2)-qcd. *Universe*, 2021. doi:10.3390/universe7050130. URL <http://doi.org/10.3390/universe7050130>.
- ⁴⁷Jeroen C. Vink and Uwe-Jens Wiese. Gauge fixing on the lattice without ambiguity. *Phys. Lett.*, B289: 122–126, 1992.
- ⁴⁸C. Alexandrou, P. de Forcrand, and M. D’Elia. The role of center vortices in QCD. *Nucl. Phys.*, A663: 1031–1034, 2000.
- ⁴⁹P. de Forcrand and M. Pepe. Center vortices and monopoles without lattice Gribov copies. *Nucl. Phys.*, B598:557–577, 2001.
- ⁵⁰Manfried Faber, Jeff Greensite, and Stefan Olejník. Direct laplacian center gauge. *Journal of High Energy Physics*, 2001(11):053–053, nov 2001. doi:10.1088/1126-6708/2001/11/053. URL <https://doi.org/10.1088/1126-6708/2001/11/053>.
- ⁵¹Manfried Faber, Jeff Greensite, and Štefan Olejník. Center dominance recovered: Direct laplacian center gauge. *Nuclear Physics B - Proceedings Supplements*, 106-107:652–654, mar 2002. doi:10.1016/s0920-5632(01)01805-9. URL [https://doi.org/10.1016/s0920-5632\(01\)01805-9](https://doi.org/10.1016/s0920-5632(01)01805-9).
- ⁵²V.G. Bornyakov, D.A. Komarov, and M.I. Polikarpov. P-vortices and drama of gribov copies. *Physics Letters B*, 497(1-2):151–158, Jan 2001. ISSN 0370-2693. doi:10.1016/s0370-2693(00)01309-5. URL [http://dx.doi.org/10.1016/S0370-2693\(00\)01309-5](http://dx.doi.org/10.1016/S0370-2693(00)01309-5).
- ⁵³G. E. P. Box and Mervin E. Muller. A Note on the Generation of Random Normal Deviates. *The Annals of Mathematical Statistics*, 29(2):610 – 611, 1958. doi:10.1214/aoms/1177706645. URL <https://doi.org/10.1214/aoms/1177706645>.
- ⁵⁴G. S. Bali, K. Schilling, and C. Schlichter. Observing long color flux tubes in SU(2) lattice gauge theory. *Phys. Rev. D*, 51:5165, 1995. doi:10.1103/PhysRevD.51.5165.
- ⁵⁵R. Höllwieser, M. Faber, J. Greensite, U. M. Heller, and Š. Olejník. Center vortices and the dirac spectrum. *Physical Review D*, 78(5), sep 2008. doi:10.1103/physrevd.78.054508. URL <https://doi.org/10.1103/physrevd.78.054508>.
- ⁵⁶H.J. Rothe. *Lattice Gauge Theories: An Introduction (Third Edition)*. World Scientific Lecture Notes In Physics. World Scientific Publishing Company, 2005. ISBN 9789813102095. URL <https://books.google.at/books?id=W-47DQAAQBAJ>.
- ⁵⁷M. Luscher, K. Symanzik, and P. Weisz. Anomalies of the Free Loop Wave Equation in the WKB Approximation. *Nucl. Phys. B*, 173:365, 1980. doi:10.1016/0550-3213(80)90009-7.
- ⁵⁸Roman Höllwieser, Francesco Knechtli, Tomasz Korzec, Michael Peardon, and Juan Andrés Urrea-Niño. Constructing static quark-anti-quark creation operators from laplacian eigenmodes. 2022. doi: 10.48550/ARXIV.2212.08485. URL <https://arxiv.org/abs/2212.08485>.
- ⁵⁹Roman Höllwieser, Francesco Knechtli, and Mike Peardon. The static energy of a quark-antiquark pair from Laplacian eigenmodes. In *39th International Symposium on Lattice Field Theory*, 9 2022.
- ⁶⁰Roman Höllwieser, Francesco Knechtli, and Mike Peardon. The static potential using trial states from Laplacian eigenmodes. *EPJ Web Conf.*, 274:02008, 2022. doi:10.1051/epjconf/202227402008.